Streamlined Discovery of Antifungal Compounds in Costa Rican Piper Species Using Weighted Gene Correlation Network Analysis of crude ^{1}H NMR Data

Celso R. Oliveira,[2] Megan J. Burroughs,[1] Lora A. Richards,[3] Lee A. Dyer,[3] Federico Urbano-Muñoz,[4] Camryn Lee,[4] Megan Warner,[4] Ian S. Wallace,[4,5] Craig D. Dodson,[1] Christopher S. Jeffrey[1]

[1]Hitchcock Center for Chemical-Ecology and Department of Chemistry, University of Nevada—Reno, Reno, NV 89557-0216

[2]University of Wisconsin—Madison, Department of Forestry and Wildlife Ecology, Madison, WI 53706

[3]Hitchcock Center for Chemical-Ecology and Department of Biology, University of Nevada—Reno, Reno, NV 89557-0216

[4]Department of Biochemistry and Molecular Biology, University of Nevada, Reno- Reno, NV 89557

[5]Complex Carbohydrate Research Center, University of Georgia, Athens, GA 30606

*Christopher S. Jeffrey, cjeffrey@unr.edu

ABSTRACT The discovery of bioactive natural products is hindered by bottlenecks encountered during the isolation, characterization, and confirmation of the active compounds. We have applied a weighted

gene correlation network analysis (WCGNA) to identify groups of ^{1}H resonances associated with bioactivity directly from crude ^{1}H NMR spectra of metabolites extracted from various *Piper* species from Costa Rica. Our screening of 30 methanolic leaf extracts against *S. cereviseae* revealed that three *Piper* species produce compounds that exhibit prominent antifungal activity. By incorporating known structural motifs into the ^{1}H NMR networks of crude extracts, we could approximate general structural types of some of the bioactive compounds during the initial phases of this targeted approach. Using unique resonances that correlated with antifungal activity, we isolated and characterized four novel compounds, three of which were identified as the active antifungal components of the mixtures. Subsequent growth inhibition assays with purified or synthetic compounds validated their efficacy, demonstrating the potential of this approach. Overall, this method reduces the need for repeated biological assessments of fractions in a traditional bioassay-guided isolation, making it a streamlined approach to identify bioactive natural products that can be used in a variety of applications.

Introduction

Plant derived natural products are a key source of molecular diversity, and they have historically driven the drug discovery enterprise.[1] The quest for new biorelevant natural products is largely centered on the implementation of bioassay-guided strategies, where bioactive plant extracts are exhaustively fractionated and assayed until one or a few target compounds can be identified as the source of activity in the original mixture. However, challenges surrounding this approach include the necessity of repeated screening throughout the isolation process, the demanding process of characterizing new compounds, and the frequent re-discovery of known natural products with established modes of action. These challenges have discouraged bioprospecting efforts and hamper our understanding of chemically mediated ecological interactions. Recent technological advances, such as the development high-throughput analytical instrumentation, multi-omics mining tools for target compound identification, and mode of action-specific bioassays, have overcome some of these limitations and re-established natural products as a source of potential therapeutics.[2-9] Despite these advances, there remains a pressing need to develop methods that

quickly guide the isolation of the functional components in complex mixtures. Network based approaches, including compound activity mapping have demonstrated remarkable efficiency for identifying target mass spectral features in microbial extracts.[10-13] Recently, we reported the development of a ^{1}H NMR-based network analysis (WCGNA) approach to identify collections of ^{1}H NMR resonances (modules) that reflect patterns of metabolites and/or structural features in complex mixtures of compounds.[14] This approach has been successfully applied for the identification of metabolic changes resulting from ecological factors or treatments, and to evaluate structure level differences in secondary metabolism across taxa.[15, 16] Previously, we assessed a diverse collection of crude *Piper* extracts to survey their growth inhibitory capabilities against four organisms, each serving as a proxy for different facets of common plant-pathogen interactions. Given that our ^{1}H NMR network-based approach is useful for the direct identification of spectral features, we envisioned that it could be applied within the biological screening framework to rapidly guide the discovery of bioactive natural products that are relevant to plant-mediated trophic interactions. This approach offers the opportunity to further accelerate the discovery of bioactive natural products by targeting the ^{1}H NMR resonances affiliated with the biological activity of the crude extracts, thereby overcoming the bottleneck of repeatedly assaying fractions throughout the isolation process to track bioactive compounds.
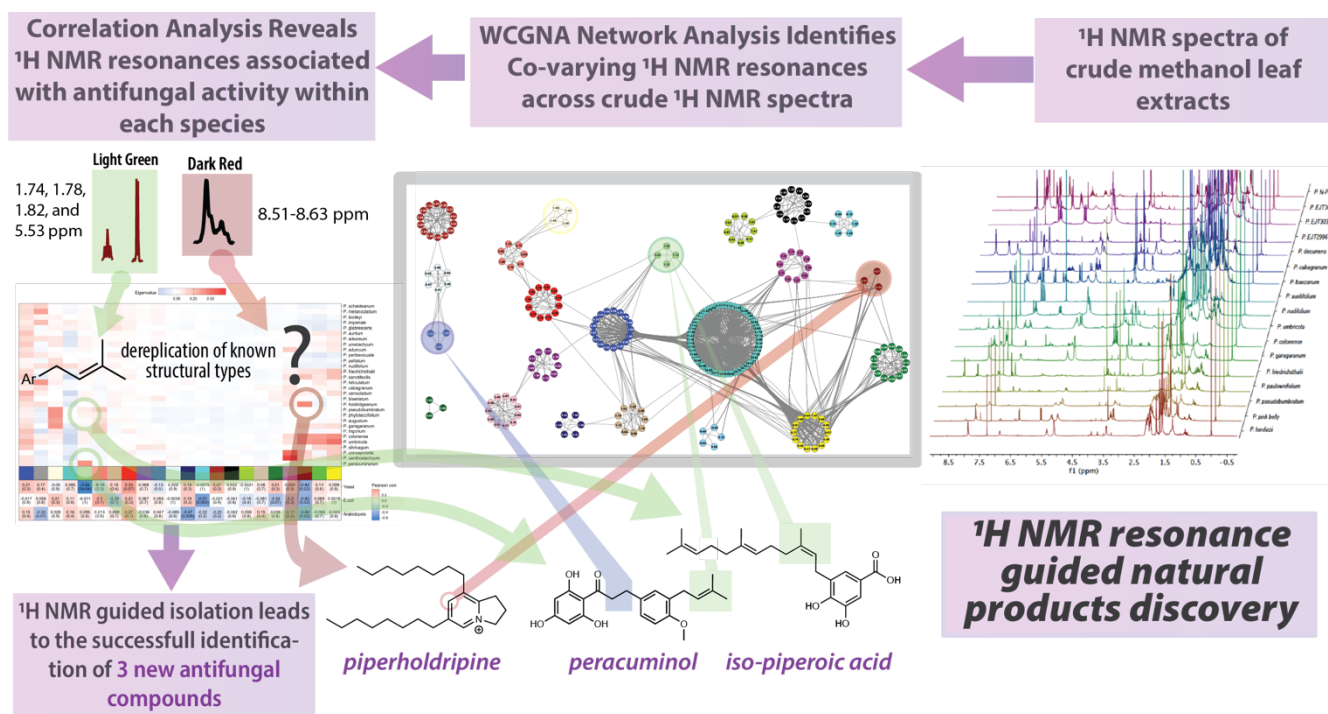
Figure 1. Summary of workflow for the ^{1}H NMR guided isolation of bioactive natural products. Our development of this approach focused on evaluating the antimicrobial activity of the crude extracts from 30 species of the plant genus *Piper* (*Piperaceae*). With over 2,500 accepted species distributed pantropically and an astounding phytochemical diversity, *Piper* is a formidable model genus for the study of ecological interactions.[17-20] However, the investigation of plant-pathogen interactions in this genus has remained mostly limited to the characterization of specific antifungal compounds across individual species. A recent review highlighted the prevalence of amides and phenylpropanoids as the most common type of antifungal compounds in the genus, which could indicate the conservation of specific modes of chemical defenses.[21, 22] In this study, we paired the ^{1}H NMR network approach with growth-inhibition assays against the model unicellular fungus *Saccharomyces cerevisiae* to guide the discovery of antimicrobial natural products that likely play a central role in plant-fungal interactions. Moreover, by seeding the networks with ^{1}H NMR spectra of known compounds, we were able to annotate structural features to the active targets prior to isolation and verification of the biological activity. Our approach ultimately led to the discovery of three new antifungal compounds, one of which demonstrated remarkably potent inhibitory activity and contained a novel imidazolium heterocyclic motif that is very rare amongst plant species and represents a new class of compound isolated from *Piper*.

Results and Discussion

Integration of ^{1}H NMR-based Network and Bioassays

Methanolic extracts from 30 different *Piper* species were screened for their ability to inhibit growth of four different organisms.[23] The metabolites in these extracts exhibited species-dependent growth inhibitory activity against *S. cereviseae* (Figure S-1) when assayed at a consistent concentration of 80 μg/mL. While most extracts displayed less than 20% inhibition, metabolite extracts from two species–*P. holdrigeanum* and *P. peracuminatum*–presented nearly total growth inhibition, followed by *P. pseudobumbratum* with 63% inhibition. These results suggested that common metabolites shared by *Piper* species are not likely to possess antifungal activity, while extracts from these three *Piper* species potentially contain one or more metabolites that cause *S. cerevisiae* growth inhibition. Leveraging this distribution of inhibitory activity, we performed a network analysis with the ^{1}H NMR spectra of the crude extracts to identify unique resonances associated with bioactive targets of the three most potent extracts. Briefly, resonance signals (nodes) were grouped into network modules according to their correlation patterns across the spectral collection. By calculating module associations with each *Piper* species (eigenvalue, ε), and module correlations with measurement of inhibitory activity (Pearson correlation, r), we could infer which modules were directly connected to the bioactivity of the crude extracts. Next, we seeded the network analysis with the ^{1}H NMR spectra obtained from a library of known natural compound mixtures, from which we calculated module correlations with the relative concentration of the mixture components. This feature allowed us to identify the structural motifs depicted by each module, which ultimately guided the elucidation and accurate isolation of the biologically active molecules.
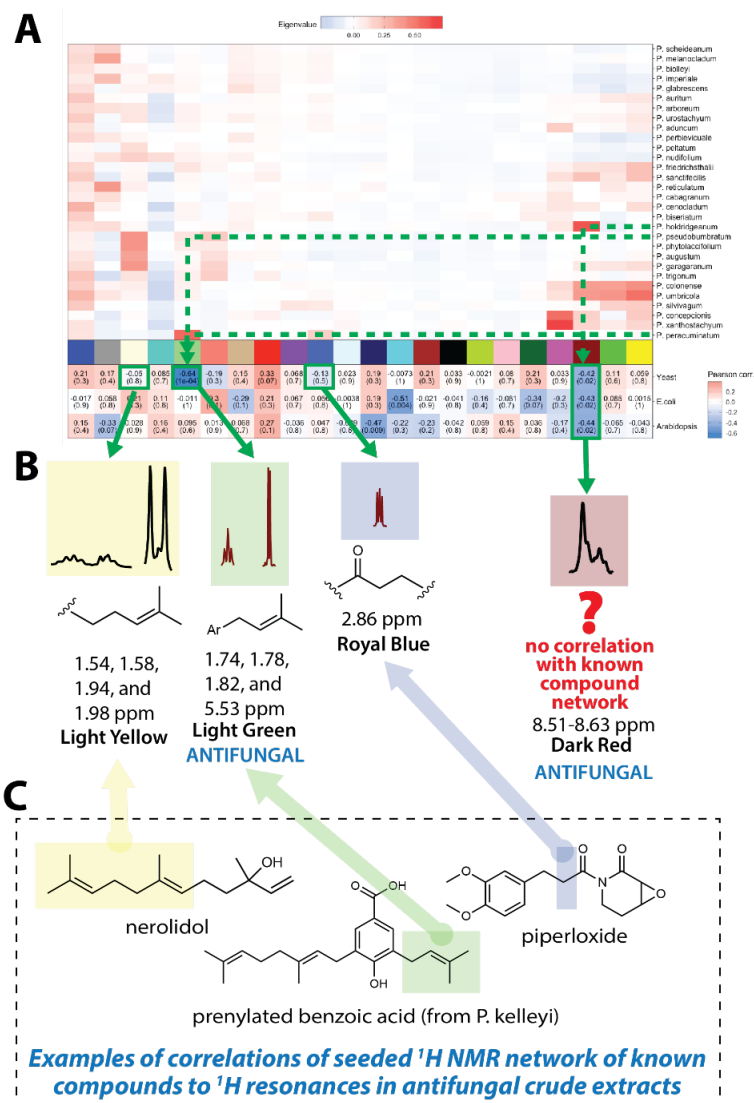
Figure 2: Module relationships obtained from the ¹H NMR network analysis of Piper extracts. A: The top heatmap panel displays module eigenvalues for each plant species and the bottom panel indicates module correlation to measurements of organismal growth across the assay panels, where negative correlations indicate an inhibitory effect. Modules are represented by colors in the middle panel. Green directional arrows denote the most important module affiliations for extracts with enhanced inhibitory activity against *S. cerevisiae*. B: Representative ¹H NMR resonances for the modules associated with bioactive extracts (light yellow, light green, royal blue, and dark red) are also shown along with tentative structural assignments based upon the seeded spectra of standard compounds. C: Example correlations between network modules of known compounds and those from crude extracts indicating that the prenyl functionality (light green) is correlated with antifungal activity. Further structural inferences were drawn from correlations of nerolidol terpene chain (light yellow) and the phenethylene functionality of

pipleroxide (royal blue). No correlations between the seeded network and the resonances of the dark red module affiliated with the inhibitory activity of the extract of Piper holdridgeanum are indicative of a new antifungal functionality not represented in our seeded network of known compounds.

The ^{1}H NMR-based network generated from the spectra of crude extracts resulted in 22 modules from all 30 spectra, with an average of 8 ($\pm$ 4) nodes/module, excluding the turquoise module which was exceedingly large for containing unspecific resonances from the δ_H 9.5–12 region. Significant correlations ($p < 0.05$) between module eigenvalues and biological activity were verified for two modules, reflecting strong associations between specific ^{1}H resonances and *Piper* species that displayed enhanced inhibitory activity (Figure 2). For instance, module light green had the strongest association with fungal inhibition ($r = 0.64$), and its highest eigenvalue was calculated for *P. peracuminatum* ($\varepsilon = 0.56$), the most potent extract against *S. cerevisiae*. The second highest eigenvalue for this module was verified with *P. pseudobumbratum* ($\varepsilon = 0.11$), which also showed moderate *S. cerevisiae* growth inhibition. Remarkably, the second most potent extract, from *P. holdrigeanum*, was associated with a different module that displayed significant correlation with inhibitory activity (dark red, $r = 0.42$, $\varepsilon = 0.62$), suggesting a structurally different molecule that was responsible for antifungal activity.

By integrating a mixture of known compounds that contain structural types known to be derived from *Piper* species into this network, we were able to directly annotate some structural features to each module, as shown in Figure 3. Thus, module light green was strongly associated with prenylated benzoic acid, and according to its chemical shifts (δ_H 5.33 for the isoprenyl C-H, δ_H 1.82–1.74 for the allylic methylenes), it described the prenyl portion of that molecule. These ^{1}H spectral features were present in both *P. peracuminatum* and *P. pseudobumbratum*, where they represented very dominant signals in the spectrum, suggesting that the corresponding target compounds were major components of each extract. Given the limited degree of structural overlap revealed by light green, we turned to other modules correlated with these *Piper* species to gain more information about the bioactive targets. The second most important

module for *P. peracuminatum*, royal blue ($\varepsilon = 0.18$), had weak correlation with yeast inhibition (r = 0.13) and was associated with pipleroxide and alkene amide in the mixtures through the phenethyl ketone proton resonance (δ_H 2.86). *P. pseudobumbratum* was most strongly associated with the module light yellow ($\varepsilon = 0.41$), which was not correlated with antifungal activity and contained chemical shifts representative of the vinylic methyl and allylic methylene resonances from nerolidol and carene in the mixtures (δ_H 1.98–1.94 and 1.58–1.54). With the convergence of these results, we predicted that these two species of *Piper* contained structurally similar prenylated aryls as their most bioactive compounds.

The module dark red, which was diagnostically associated with the antifungal activity of *P. holdrigeanum*, contained a unique set of resonances at the narrow range of δ_H 8.53-8.62. We did not encounter informative associations with any compound structural features of the seeded mixture that could aid in a preliminary characterization of the target compound, suggesting that this molecule was structurally distinct from any of the reference compounds used. This result demonstrates that the ^{1}H NMR network approach could help to identify novel molecular space and dereplicating at an early stage of analysis. Unlike the other resonances correlating with bioactivity from the crude ^{1}H NMR spectra of *P. peracuminatum* and *P. pseudobumbratum* extracts, this compound was also a minor component of the crude extract. The ability for this approach to identify even minor ^{1}H NMR resonances that were affiliated with the biological activity of the extract and that were not affiliated with any training set resonances suggested that the *P. holdridgeanum* extract contained a potent antifungal that is structurally distinct from other compounds isolated from Piper. We thus considered the characteristic resonances represented by modules light green and dark red to perform an ^{1}H NMR resonance-guided fractionation of the crude extracts and isolate the active compounds from *P. peracuminatum, P. pseudobumbratum*, and *P. holdrideganum*.

Compound isolation and structure determination

To isolate the compounds that correlated to the bioactivity, we adopted a general isolation protocol that minimized the number of fractions and the necessity of repeated bioactivity screening by tracking the

target compounds through ^{1}H NMR analysis. The crude methanolic extracts were pre-fractionated using a SepPak C18 column eluted with 50-100% acetone:water. Fractions were analyzed by ^{1}H NMR and those containing the target resonances were then prioritized for further purification via reverse-phase preparatory HPLC. The isolated compounds were screened against *S. cereviseae* to confirm inhibitory activity and subsequently analyzed using various 2D NMR techniques for structural characterization.

  Initial fractionation of the *P. pseudobumbratum* extract yielded the target compound at high concentration from the chromatographic fraction eluted with 50% acetone:water. Further purification of this extract provided 35 mg of compound **1** with an ESIHRMS *m/z* 357.2009 (calculated for $C_{22}H_{30}O_4$, 357.2071 [M - H]⁻), and which displayed the signature resonances from module light green. Analysis of the ^{1}H NMR data suggested the presence of a 1,2,3,5-tetrasubstitued aromatic ring with a single farnesyl substituent, which was characterized by the presence of three vinylic resonances (δ_H 5.07, 5.16 and 5.36) and the single benzylic methylene (δ_H 3.33). From the ^{13}C NMR data we concluded that one of the ring substituents was a carboxylic acid (δ_C 170.6 ppm) with the other two assigned as phenolic hydroxyl groups given the presence of two oxygenated aryl carbons (δ_C 149.4 and 145.4). Finally, we concluded that both aromatic protons H-2 and H-6 were ortho to the carboxylic acid since they displayed ^{1}H{^{13}C} HMBC correlations with the carboxylic carbon (C-7) and one of the hydroxylated carbons (C-4), and the observed chemical shift values at δ_H 7.34 and 7.48 were consistent with this substitution pattern. NOESY data confirmed the configuration of the alkene groups, and the final structure was determined as (2'*Z*,6'*E*,10'*E*)-piperoic acid (**1**), which is a new isomeric form of the equivalent (2'*E*,6'*Z*,10'*E*) compound isolated from *P. auritum*.[24]

**Table 1. ^{1}H and ^{13}C NMR assignments for (2'*Z*,6'*E*,10'*E*)-piperoic acid (1)**
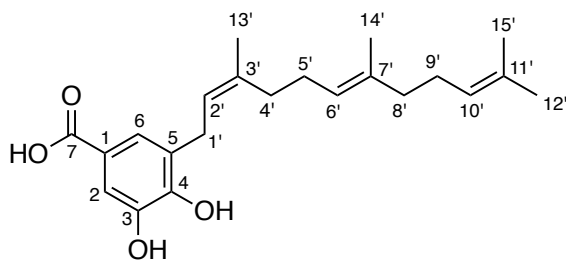
Position	δ_C, type	δ_H	HMBC	NOESY
1	122.4, C			
2	115.1, CH	7.32 d (2.0 Hz)	3, 4, 6, 7	
3	145.4, C			
4	149.4, C			
5	137.3, C			
6	124.1, CH	7.35 dt (2.0, 0.5 Hz)	2, 4, 7	1', 2'
7	170.7, C			
1'	28.8, CH_2	3.33 br d (7.1 Hz)	4, 5, 2', 3'	6, 4'
2'	124.0, CH	5.36 br t (7.4 Hz)	1', 3', 4', 13'	6, 13'
3'	129.0, C			
4'	32.9, CH_2	2.21–2.15	5, 2', 5', 6', 13'	1', 6', 13'
5'	27.6, CH_2	2.16–2.09	4', 6', 7'	14'
6'	125.3, CH	5.16 br t (7.4 Hz)	5', 8', 14'	4', 8'
7'	136.2, C			
8'	40.8, CH_2	1.98–1.92	5', 6', 7', 9', 10', 14'	6', 14'
9'	27.8, CH_2	2.08–2.01	6', 8', 10', 11'	14'
10'	125.5, CH	5.07 m	12', 15' (weak)	8', 12'
11'	132.0, C			
12'	25.9, CH_3	1.65 br s	10', 11', 12'	10'
13'	23.8, CH_3	1.75 br q (1.2 Hz)	5, 2', 3', 4'	2', 4'
14'	16.1, CH_3	1.60 br s	6', 7', 8'	5'
15'	17.7, CH_3	1.58 br s	10', 11', 15'	

Solid-phase partitioning of the *P. peracuminatum* extract led to the recovery of the target peaks in the fractions eluted with 50% and 60% acetone:water. These fractions were pooled for purification and the resulting collections yielded two novel compounds–**2** (20 mg) and **3** (16 mg)–with proximal eluting times that contained the target resonances. Compound **2** resulted in an ESIHRMS *m/z* 355.1560 (calculated for $C_{21}H_{24}O_5$, 355.1551 [M - H]⁻) and compound **3** yielded an ESIHRMS *m/z* 409.2030 (calculated for $C_{25}H_{30}O_5$, 409.2020 [M - H]⁻). Both compounds presented resonances characteristic of prenyl groups (identified by the light green module) across the ¹H NMR spectrum, but they were consistently and slightly shifted upfield for **3** (Table 4) compared to the same peaks in **2** (Table 3). The compounds also had the signature peak from module royal blue (δ_H 2.86, H-9), which was confirmed to be the part of a

propenone moiety based on its ^{1}H{^{1}H} COSY correlations with the methylene resonance at ~δ_H 3.25 (H-8), and on the ^{1}H{^{13}C} HMBC peaks of both methylene resonances with the ketone resonance at δ_C 205.9 (C-7). The peak from H-9 was present at an integration ratio of 1:1 with the vinylic resonance (~δ_H 3.25, H-2') in compound **3**, which led us to the conclusion that this compound possessed two equivalent prenyl groups. The most distinctive proton peak patterns for the two compounds were verified in the aromatic region, where compound **2** displayed three diagnostic resonances for a 1,2,4-trisubstituted ring, while **3** contained a unique singlet indicative of a symmetric 1,2,3,4-tetrasubstituted ring. We confirmed from the ^{1}H{^{13}C} HMBC correlations between these aromatic protons and the carbons C-9 and C-1' that the prenyl groups were implicated in the symmetry of the aromatic ring of **3**, and that in both compounds the propenone moiety was attached to the ring through the β-carbonyl carbon and meta position relative to the prenyl groups. The presence of an oxygenated aryl carbon (C-13) in both compounds led to the conclusion that the remaining substituent was a hydroxyl group in compound **3** and a methoxyl group in **2** (δ_H 3.77, H-16). Finally, we identified the singlet at δ_H 5.86 as being part of an acylphloroglucinol aromatic moiety, which was connected to the propenone linker through the carbonyl carbon (^{1}H{^{13}C} HMBC, C-7 and H-3/5), thus defining the structures of peracuminol (**2**) and 14-prenylperacuminol (**3**) (Tables 2 and 3, respectively).
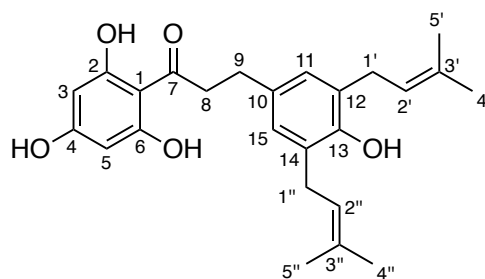
Table 2. ^{1}H and ^{13}C NMR assignments for peracuminol (2)
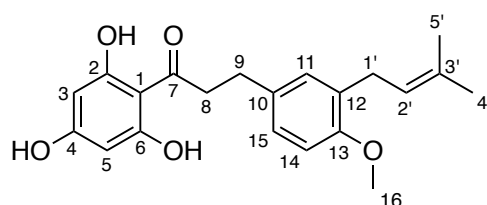
Position	δ_C, type	δ_H	HMBC
1	105.3, C		
2/6	165.2, C		
3/5	95.9, CH	5.86 s	1, 2/6, 4, 7
4	164.9, C		
7	205.9, C		
8	46.8, CH$_2$	3.27–3.24	7, 9, 10

Position	δ_C, type	δ_H	HMBC
9	30.5, CH_2	2.84 dd (8.2, 6.7 Hz)	7, 8, 10, 11, 15
10	134.7, C		
11	130.4, CH	6.98 d (2.0 Hz)	9, 13, 15, 1'
12	130.6, C		
13	156.6, C		
14	111.5, CH	6.82 d (8.3 Hz)	10, 11, 12, 13, 15
15	127.6, CH	7.01 dd (8.2, 2.3 Hz)	11, 13, 14
16	56.1, CH_3	3.77 s	
1'	29.3, CH_2	3.24 br d (7.4 Hz)	11, 12, 13, 2', 3'
2'	123.7, CH	5.25 m	5' (weak)
3'	132.9, C		
4'	25.9, CH_3	1.70 br s	2', 3', 5'
5'	17.8, CH_3	1.70 br s	2', 3', 4'

Table 3. ^1H and ^{13}C NMR assignments for 14-prenylperacuminol (3)

Position	δ_C, type	δ_H	HMBC
1	105.3, C		
2/6	165.1, C		
3/5	95.8, CH	5.86 s	1, 2/6, 4, 7
4	164.7, C		
7	206.0, C		
8	46.7, CH_2	3.21–3.27	7, 9, 10
9	30.6, CH_2	2.79 t (7.6 Hz)	7, 8, 10, 11/15
10	134.4, C		
11/15	128.2, CH	6.79 s	9, 13, 1'/1"
12/14	128.7, C		
13	151.0, C		
1'/1"	29.7, CH_2	3.25 br d (7.3 Hz)	11/15, 13, 12/14, 2'/2", 3'/3", 5'/5"
2'/2"	125.5, CH	5.26 m	1'/1", 4'/4", 5'/5"
3'/3"	132.0, C		
4'/4"	23.8, CH_3	1.72 br s	2'/2", 3'/3", 5'/5"
5'/5"	17.7, CH_3	1.71 br s	2'/2", 3'/3", 4'/4"

12

Initial attempts to purify the bioactive component(s) from *P. holdrigeanum* were met with failure, only resulting in a prenylated benzoic acid derivative (**5**, Supporting Information) that did not contain the targeted resonances from module dark red and demonstrated no antifungal activity. We found that silica gel chromatography was not amenable to the isolation of the targeted resonances and speculated that the lack of a strong chromophore also limited the application of traditional isolation methods using reverse-phase media with UV detection. By employing reverse phase prep-HPLC with MSD detection to partition the crude extract, we recovered 10 fractions containing varying concentrations of the compound(s) exhibiting the target resonances (δ_H 8.17 and 8.61). All of these fractions exhibited potent antifungal activity against *S. cerevisiae* and contained a component with *m/z* 344.3320 corresponding to $C_{24}H_{42}N^+$ (calculated for 344.3312 $[M]^+$). Further purification of the pooled fractions led to a highly enriched fraction of the target compound containing the two broad singlets identified by module dark red along with a propenyl system [δ_H 4.81 (t), 2.48 (pent), and 3.44 (t), coupled via COSY], and two long-chain aliphatic systems. The diagnostic ${}^1H$ NMR resonances at ~δ_H 8.6 indicated the presence of a pyridinium moiety, and ${}^{13}C$ NMR analysis further demonstrated the presence of 5 aromatic carbon resonances (Table 4). HMBC analysis confirmed the connectivity of the substituents to the aromatic ring, which supported the assignment of the novel C6,C8-*bis*-octyl substituted 2,3-dihydro-1*H*-indolizidinium alkaloid, piperholdripine (**4**), as the principal bioactive compound of the crude mixture with the ${}^1H$ NMR resonance for the C-2 pyridinium methine as a strong indicator of bioactivity for the crude extract of *Piper holdridgeanum* (Figure 3).

Table 4. ${}^1H$ and ${}^{13}C$ NMR assignments for piperholdripine (4)
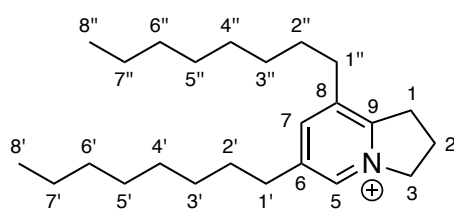
Position	δ_C, type	δ_H	HMBC
1	31.6, CH_2	3.47 t	8, 9

2	22.1, CH$_2$	2.50 t	1,3,9
3	60.5, CH$_2$	4.83 t	1,2,5,9
4	N		
5	138.8, CH	8.60 br s	6,7,9
6	142.9, C		
7	145.9, C	8.17 br s	5,9
8	140.7, C		
9	156.6, C		
1'/1"	33.0, CH$_2$	2.80 t (7.3 Hz)	2'/2", 5, 6, 7, 8, 9
2'/2"	31.7, CH$_2$	1.69, 1.70 m	8, 6, 1'/1", 3'/3"-7'/7"
3'/3"-4'/4"	30.2, 30.1, CH$_2$	1.34-1.44	
5'/5"-7',7"	32.7, 33.2, 23.6, CH$_2$	1.26-1.36	
8'/8"	14.3 CH$_3$	0.90 m	

Comparison of the ^{1}H and ^{13}C NMR data this compound to other naturally occurring and synthetic 2,3-dihydro-1*H*-indolizidinium alkaloids, specifically the C6,C8-*bis*-heptyl synthetic analog prepared by a biomimetic Chichibabin pyridine synthesis reported by Snider and co-workers,[25] further validated the proposed structure. This finding underscores the efficacy of the network-based ^{1}H NMR approach in identifying biologically relevant resonances and rapidly isolating bioactive compounds that would otherwise remain concealed due to complex interactions between multiple organisms.

HMBC correlations   ^{1}H ^{1}H-COSY correlations

piperhodripine (**4**)

- -
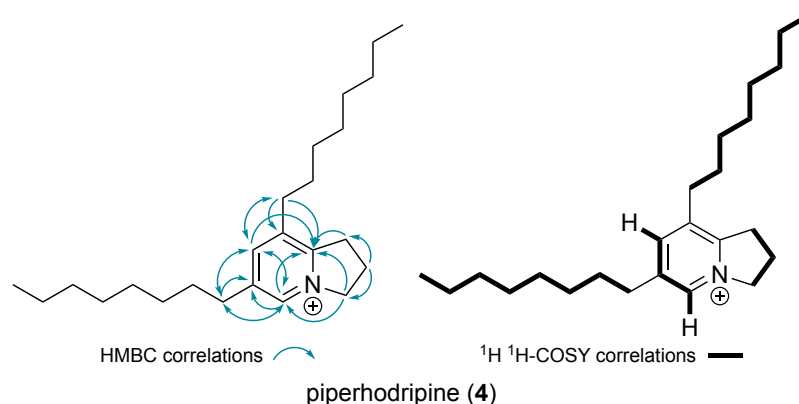
Synthesis of piperholdripine (**4**) based upon Snider *et al.*

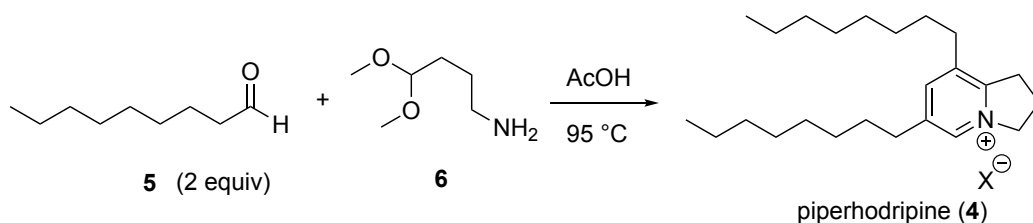**5** (2 equiv)   **6**   AcOH 95 °C   piperhodripine (**4**)

Figure 3. Key 2D NMR correlations and confirmatory synthesis leading to the structure determination of piperholdripine (4)

Bioactivity of the isolated compounds

The purified compounds were subjected to *S. cerevisiae* growth inhibition assays to investigate their antifungal properties. We first assayed the isolated compounds from *P. pseudobubratum* and *P. peracuminatum* at a standard concentration of 100 μM in *S. cerevisiae* growth inhibition assays as described in Materials and Methods (Figure 4; A and B). Compound **1** from *P. pseudobumbratum* inhibited *S. cerevisiae* growth by 25% compared to untreated or solvent controls. In contrast, *P. peracuminatum* compound **2** inhibited *S. cerevisiae* growth by 75%, and cells treated with this compound exhibited markedly extended lag phase growth compared to untreated cells. Dose-response analysis of cells treated with *P. percuminatum* compound **2** indicated an IC$_{50}$ of 10.5 μM (Figure 4; C). *P. peracuminatum* compound **3** was less active at 100 μM compared to compound **2**, displaying only 40% growth inhibition compared to untreated controls. These results suggest that the prenyl moiety captured by module light green is a determining structural feature for compound activity in the investigated extracts, which is further supported by reports that identify prenylated benzoic acid derivatives with antifungal activity across several species of *Piper*.[14] It is noteworthy that although this structural feature was correlated with increased inhibitory activities of compounds **1** and **2**, the presence of a second prenyl unit in 14-prenylperacuminol (**3**) resulted in significantly reduced potency, suggesting a structural specificity affiliated with *S. cerevisiae* inhibition. Moreover, the enhanced inhibitory effect of *P. peracuminatum* compound **2** was associated with another module (royal blue) that represented part of the dihydrochalcone motif, which is also present in antifungal compounds isolated from *P. mollicomum*[15] and *P. aduncum*[16], and that can be postulated as an important structural determinant for yeast inhibition. Conversely, the module that was most strongly associated with *P. pseudobumbratum* (light yellow) was not correlated with inhibitory activity as it represented structural features of an elongated farnesyl group that were not as determining for inhibitory activity.
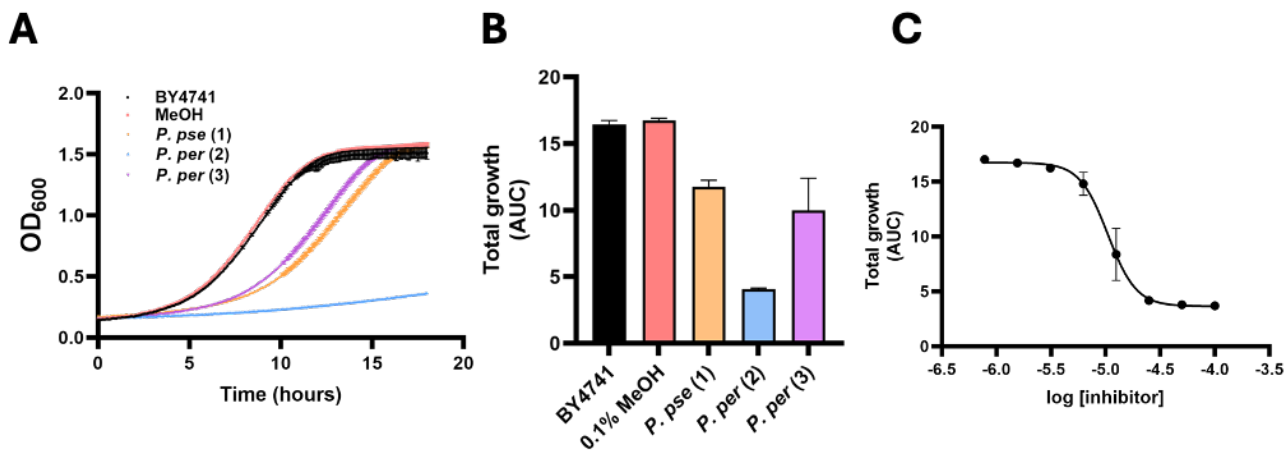
Figure 4. Antifungal activity of P. *pericuminatum* and *pseudobumbaratum* compounds. Purified compounds were assayed against *S. cerevisiae* BY4741 as described in Materials and Methods at a concentration of 100 µM. *S. cerevisiae* treated with 0.1% MeOH served as a solvent control. **A.** Representative growth curves of *S. cerevisiae* BY4741 treated 100 µM *P. pseudobumbratum* compound 1 (orange), *P. pericuminatum* compound 2 (blue), or *P. pericuminatum* compound 3 (purple) compared to 0.1% MeOH (red) and untreated (black) growth curves. Error bars represent SEM (n = 3). **B.** AUC values of integrated growth curves are shown for similar experiments. Error bars represent SEM (n = 3). **C.** *P. pericuminatum* compound 2 was assayed at decreasing concentrations to establish a dose-response relationship. Error bars represent SEM (n = 3).

The antifungal activity of *P. holdridgeanum* extracts (Figure 5; A, B) revealed an inhibitory effect comparable to that observed for *P. peracuminatum* but originating from a compound that was present at a considerably lower concentration according to the target resonances depicted by the network analysis. Synthesis of piperholdripine (**4**) using the methods described by Snider and co-workers yielded a product spectroscopically identical to the isolated compound and demonstrated the strong antifungal activity, inhibiting *S. cerevisiae* growth by greater than 80% compared to untreated and solvent controls (Figure 5A, B). Dose-response analysis of piperholdripine (**4**) growth inhibition activity indicated an IC_{50} of 4.9 µM (Figure 5; C).
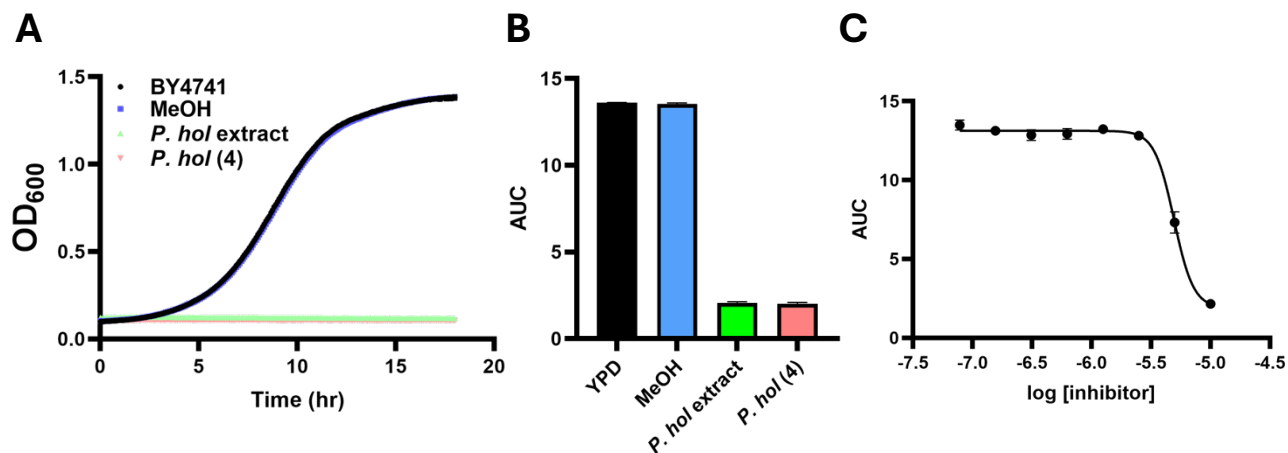
Figure 5. Growth inhibition analysis of purified piperholdripine (4): *S. cerevisiae* BY4741 was grown as described in Materials and Methods in YPD medium supplemented with 80 μg/ mL *P. holdrigeanum* extract, 100 μM purified compound 4, or 0.1% MeOH as a negative control for 18 hours at 30°. **A.** Representative growth curves of samples are shown. **B.** The area under growth curves was calculated and plotted. Error bars represent SEM (n = 3 biological replicates, 9 technical replicates). **C.** Dose-response curves of *S. cerevisiae* cultures subjected to decreasing concentrations of piperholdripine (**4**).
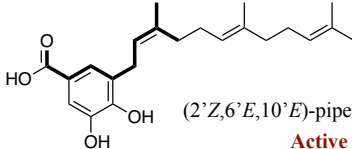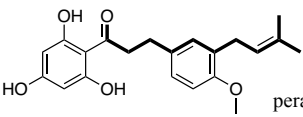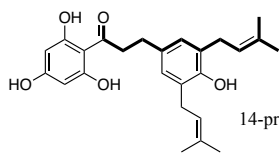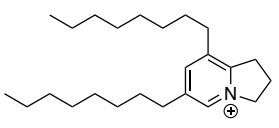
We predict that the evaluation of a larger library of *Piper* extracts using this methodology may further elucidate the structural effects (e.g., elongation and functionalization of the prenyl chain) in modulating the antifungal activities of these compounds and to guide the isolation of novel molecular structures associated with biological activity. Complementarily, the application of this approach with yeast deletion collections could provide a powerful method to identify the specific mechanisms of action of a compound.[17] Gene knockouts that result in altered drug resistance may offer direct clues to structure-cellular target affiliations, and thus help to discern whether varying levels of inhibition result from differentiated compound-specificity towards a common target, or if these compounds target distinct cellular processes. The refined structural information obtained from the chemical modules can then be evaluated against susceptible/resistant phenotypes to highlight the role of specific molecule motifs in dictating biological activity.

Conclusion

Overall, our ^{1}H NMR-based network approach allows the deconvolution of phytochemical profiles into quantifiable chemical characters that can be mapped directly onto bioassay data. The immediate product of this process is the identification of diagnostic peaks in the spectrum that can be utilized to guide the isolation of bioactive compounds, thus replacing the time consuming and laborious nature of recursive bioassay of chromatographic fractions. Moreover, integrating a suitable library of spectra from pure compounds in conjunction with the extracts provides a method to dereplicate known compounds through tentative annotation of crude ^{1}H NMR spectra, and a means for tailoring isolation strategies specific to the target compound structural class. However, the utility of this methodology is not limited to optimizing the process of compound isolation and identification. For example, in combination with inhibition assays against knockout libraries of model organisms, such as *S. cerevisiae*, the analysis of chemical modules can support the optimization of structural features for enhancing compound activity against specific cellular targets and for dereplicating known mechanisms of action/biomolecular targets prior to isolation. Additionally, activity screening against other species of fungi might reveal additional inhibitory compounds and provide evidence for the implication of structural features in compound selectivity towards different strains. The information contained by the modules can ultimately help assessing the taxonomical recurrence of molecular motifs associated with specific modes of biological activity, as demonstrated with the genus *Piper*, and help retracing the evolutionary history of chemical defenses in plants and other organisms. Coupled with the gamut of bioactivity and target-based assays, this methodology could be not only a valuable means to study conserved phytochemical defenses across taxa, but also a useful tool for establishing structure-activity relationships (SAR) of potential targets and optimizing the pharmacological properties of specialized metabolites.

Table 5. Growth-inhibition activity of crude extracts and isolated compounds against *S. cerevisiae*.

Species and Isolated Compound(s)	% inhibition*	IC$_{50}$ (μM)
P. pseudobumbratum	63.2	

Structure		
(2'Z,6'E,10'E)-piperoic acid (**1**) **Active**	61.3	n.d.
P. peracuminatum	98.7	
peracuminol (**2**) **Active**	79.3	10.5 µM
14-prenylperacuminol (**3**) **Not Active**	0.0	>100 µM
P. holdrigeanum	93.8	
piperholdripin (**4**) **Active**		4.9 µM

Experimental Section

Extractions

30 different species of Piper were collected at La Selva Biological Station in Costa Rica, Heredia Province (10°25′ N, 84°00′ W, 50 m). The most recently expanded leaves were collected from multiple individuals and pooled for each species. All leaf samples were dried in an air-conditioned laboratory, ground with mortar and pestle to a fine powder, and 2 g of this powder was transferred to a screw cap test tube and combined with 10 mL of methanol. The samples were sonicated for 10 minutes and filtered to separate the leaf material from the supernatant. This step was repeated a second time, and the supernatants were combined and transferred to pre-weighed 20 mL scintillation vials. The solvent was removed under reduced pressure at 25 °C and prepared for NMR analysis.

Bioassays

Crude methanolic extracts were assayed against *Saccharomyces cerevisiae* BY4741. S. cerevisiae cells were initially grown on solid YPD medium (2% [w/v] peptone, 1% [w/v] yeast extract, 2% [w/v] glucose)

and incubated for 2 days at 30 °C. A single colony was used to inoculate a 10 mL YPD culture, which was incubated at 30 °C for 18 h with shaking. Saturated cultures were diluted 100-fold into liquid YPD, and extracts or purified compounds were diluted into these cultures at indicated concentrations. Samples were arrayed into Honeycomb 100-well plates (Growth Curves USA) and assayed in a Bioscreen C plate reader (Growth Curves USA). OD_{600} readings were taken at 5 min intervals for 18 h with 30 s of shaking before each reading as previously described.[26] Following the identification of inhibitory targets, the assays were repeated with the purified compounds, initially at a concentration of 100 μM, and then at serial dilutions to calculate the half maximal inhibitory concentration (IC_{50}). Area Under Curve (AUC) values were plotted against the log of the inhibitor concentration, and IC_{50} was calculated in GraphPad Prism using the log(inhibitor) vs. response variable slope model.

^{1}H NMR analyses

Crude plant extracts were dissolved in 1 mL of methanol-d4 containing 0.03% TMS to yield a nominal concentration of 15 mg/mL, filtered to remove insoluble residues and then transferred to 5 mm NMR tubes. The samples were analyzed by ^{1}H-NMR spectroscopy using a Varian 400-MR (399.8 MHz) spectrometer with 128 transients per spectrum, 2.556 s acquisition time, and 1.0 s delay time. Spectral data was processed using MNova (version 10.0, Mestrelab Research, Santiago de Compostela, Spain). Each spectrum was individually aligned by the residual methanol peak (septet, δH 3.31), phase-corrected (global method) and baseline-corrected (polynomial fit of order 3). Following, all spectra were superimposed and binned into 0.04 ppm intervals from 12 ppm to 0.5 ppm (bins integrated by average sum). After binning the data, the solvent peak residuals were removed, the spectra were normalized to a total area of 100 units, and the resulting data was exported into a .csv file to be used in the network analysis.

Purified compounds were resuspended in methanol-d4 containing 0.03% TMS to an approximate concentration of 10 mg/mL and subjected to complete structural characterization. 1D and 2D NMR analysis was conducted on a Varian 400-MR (399.8 MHz) spectrometer using the following number of transients, 1H: 128, 13C: 15000, gCOSY: 4x128, gHSQC: 4x256 and gHMBC: 8x512. Optimal pulse

widths (pw90), delay and acquisition times were experimentally determined for each compound. In cases where the solvent residual peaks compromised the characterization of the compounds, samples were also prepared and analyzed using acetonitrile-d3 to resolve the assignments.

Network analysis

Network analysis of the crude 1H NMR spectra was performed according to previously reported methodology.[27] To facilitate the characterization of bioactive molecular targets from the crude extracts, we seeded the network analysis with spectra collected from a library of prepared mixtures of known compounds that broadly represent metabolite classes encountered in plant extracts. After the modules were calculated for the combined set of mixtures and extracts, we calculated the Pearson correlations between module eigenvalues and bioassay data. We then processed a parallel analysis to assign module correlations with compound concentrations from the mixtures. By comparing these results, we were then able to estimate the structural elements associated with the bioactive targets present in the crude extracts. Moreover, by referring to the modules that demonstrated significant correlation with bioactivity, we identified diagnostic peaks in the ^{1}H-NMR spectrum that were used as a guide for the isolation of the bioactive compounds.

[Incorporate parameters: beta=11, cutpar=0.25, 3 nodes per module, cytoTresh=0.009]

Compound isolation

For the isolation of target compounds, we sequentially and extensively extracted 6 g of leaf material with *n*-hexane, acetone and methanol at room temperature under mechanical agitation. For extracts that displayed the target peaks upon 1H NMR analysis, 200 mg of the extract were pre-fractionated using preparative reverse-phase medium pressure liquid chromatography (RP-MPLC; 10 g column, FC-C18 60 μm, 2.5 cm x 8 cm), eluted with acetone:H_2O at discrete increments of 10% acetone. Two samples of 15 mL were collected for each eluent mixture, then dried under reduced pressure, and analyzed by ^{1}H NMR. When additional steps of purification were necessary, the pre-purified fractions were submitted to RP-MPLC (5 g, FC-C18 60 μm, 1.5 cm x 5 cm), eluting with a linear gradient of acetone:H_2O from 0% acetone to 100% acetone over 30 minutes.
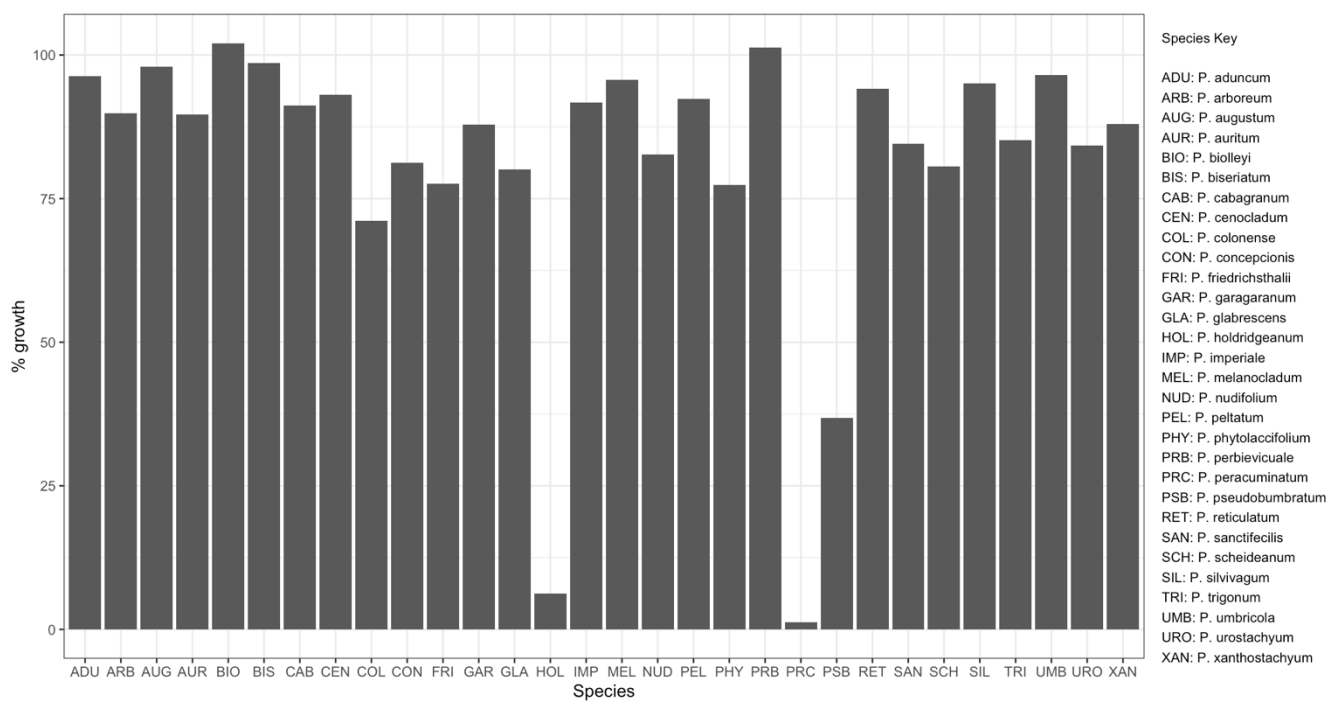
Figure S1: Growth-inhibition activity of *Piper* extracts against *S. cereviseae.* Relative yeast growth was calculated as the ratio between the area under curve (AUC) of extract assays and the control (YPD + yeast + methanol).

References Cited

(1) Atanasov, A. G.; Zotchev, S. B.; Dirsch, V. M.; Orhan, I. E.; Banach, M.; Rollinger, J. M.; Barreca, D.; Weckwerth, W.; Bauer, R.; Bayer, E. A.; et al. Natural products in drug discovery: advances and opportunities. *Nature Reviews Drug Discovery* **2021**, *20* (3), 200-216. DOI: 10.1038/s41573-020-00114-z.

(2) Gaudêncio, S. P.; Pereira, F. Dereplication: racing to speed up the natural products discovery process. *Nat. Prod. Rep.* **2015**, *32* (6), 779-810.

(3) Hight, S. K.; Clark, T. N.; Kurita, K. L.; McMillan, E. A.; Bray, W.; Shaikh, A. F.; Khadilkar, A.; Haeckl, F. P. J.; Carnevale-Neto, F.; La, S.; et al. High-throughput functional annotation of natural

products by integrated activity profiling. *Proc Natl Acad Sci U S A* **2022**, *119* (49), e2208458119. DOI: 10.1073/pnas.2208458119 From NLM Medline.

(4) Najmi, A.; Javed, S. A.; Al Bratty, M.; Alhazmi, H. A. Modern approaches in the discovery and development of plant-based natural products and their analogues as potential therapeutic agents. *Molecules* **2022**, *27* (2), 349.

(5) Kang, H.-S. Phylogeny-guided (meta)genome mining approach for the targeted discovery of new microbial natural products. **2017**, *44* (2), 285-293.

(6) Huang, B.; Zhang, Y. Teaching an old dog new tricks: Drug discovery by repositioning natural products and their derivatives. *Drug Discovery Today* **2022**.

(7) Morehouse, N. J.; Clark, T. N.; McMann, E. J.; van Santen, J. A.; Haeckl, F. P. J.; Gray, C. A.; Linington, R. G. Annotation of natural product compound families using molecular networking topology and structural similarity fingerprinting. *Nature Communications* **2023**, *14* (1), 308. DOI: 10.1038/s41467-022-35734-z.

(8) Carnevale Neto, F.; Clark, T. N.; Lopes, N. P.; Linington, R. G. Evaluation of Ion Mobility Spectrometry for Improving Constitutional Assignment in Natural Product Mixtures. *Journal of Natural Products* **2022**, *85* (3), 519-529. DOI: 10.1021/acs.jnatprod.1c01048.

(9) Adamek, M.; Alanjary, M.; Ziemert, N. Applied evolution: phylogeny-based approaches in natural products research. *Nat Prod Rep* **2019**, *36* (9), 1295-1312. DOI: 10.1039/c9np00027e From NLM.

(10) Edison, A. S.; Colonna, M.; Gouveia, G. J.; Holderman, N. R.; Judge, M. T.; Shen, X.; Zhang, S. NMR: Unique Strengths That Enhance Modern Metabolomics Research. *Analytical Chemistry* **2021**, *93* (1), 478-499. DOI: 10.1021/acs.analchem.0c04414.

(11) Jahangir, M.; Nuringtyas, T. R.; Ali, K.; Wilson, E. G.; Choi, Y. H.; Verpoorte, R. NMR-based Metabolomics: Understanding Plant Chemistry and Identification of Biologically Active Compounds. In *NMR-based Metabolomics*, Keun, H. C. Ed.; The Royal Society of Chemistry, 2018; p 0.

(12) Flores-Bocanegra, L.; Al Subeh, Z. Y.; Egan, J. M.; El-Elimat, T.; Raja, H. A.; Burdette, J. E.; Pearce, C. J.; Linington, R. G.; Oberlies, N. H. Dereplication of fungal metabolites by NMR-based compound networking using MADByTE. *Journal of natural products* **2022**, *85* (3), 614-624.

(13) Kim, H. K.; Choi, Y. H.; Verpoorte, R. NMR-based metabolomic analysis of plants. *Nature protocols* **2010**, *5* (3), 536-549.

(14) Richards, L. A.; Oliveira, C.; Dyer, L. A.; Rumbaugh, A.; Urbano-Muñoz, F.; Wallace, I. S.; Dodson, C. D.; Jeffrey, C. S. Shedding Light on Chemically Mediated Tri-Trophic Interactions: A 1H-NMR Network Approach to Identify Compound Structural Features and Associated Biological Activity. *Frontiers in Plant Science* **2018**, *9*, Methods. DOI: 10.3389/fpls.2018.01155.

(15) Uckele, K. A.; Jahner, J. P.; Tepe, E. J.; Richards, L. A.; Dyer, L. A.; Ochsenrider, K. M.; Philbin, C. S.; Kato, M. J.; Yamaguchi, L. F.; Forister, M. L.; et al. Phytochemistry reflects different evolutionary history in traditional classes versus specialized structural motifs. *Scientific reports* **2021**, *11* (1), 1-14.

(16) Decker, L. E.; Jeffrey, C. S.; Ochsenrider, K. M.; Potts, A. S.; de Roode, J. C.; Smilanich, A. M.; Hunter, M. D. Elevated atmospheric concentrations of CO2 increase endogenous immune function in a specialist herbivore. *Journal of Animal Ecology* **2021**, *90* (3), 628-640.

(17) Richards, L. A.; Dyer, L. A.; Forister, M. L.; Smilanich, A. M.; Dodson, C. D.; Leonard, M. D.; Jeffrey, C. S. Phytochemical diversity drives plant-insect community diversity. *P Natl Acad Sci USA* **2015**, *112* (35), 10973-10978. DOI: 10.1073/pnas.1504977112.

(18) Philbin, C. S.; Dyer, L. A.; Jeffrey, C. S.; Glassmire, A. E.; Richards, L. A. Structural and compositional dimensions of phytochemical diversity in the genus Piper reflect distinct ecological modes of action. *Journal of Ecology* **2022**, *110* (1), 57-67.

(19) Uckele, K. A.; Jahner, J. P.; Tepe, E. J.; Richards, L. A.; Dyer, L. A.; Ochsenrider, K. M.; Philbin, C. S.; Kato, M. J.; Yamaguchi, L. F.; Forister, M. L.; et al. Phytochemistry reflects different evolutionary history in traditional classes versus specialized structural motifs. *Sci Rep-Uk* **2021**, *11* (1). DOI: ARTN 17247 10.1038/s41598-021-96431-3.

(20) Sen, S.; Rengaian, G. A Review on the Ecology, Evolution and Conservation of Piper (Piperaceae) in India: Future Directions and Opportunities. *The Botanical Review* **2021**, *88* (3), 333-358. DOI: 10.1007/s12229-021-09269-9.

(21) Xu, W.-H.; Li, X.-C. Antifungal Compounds from Piper Species. *Current Bioactive Compounds* **2011**, *7* (4), 262-267. DOI: http://dx.doi.org/10.2174/157340711798375822.

(22) Carsono, N.; Tumilaar, S. G.; Kurnia, D.; Latipudin, D.; Satari, M. H. A Review of Bioactive Compounds and Antioxidant Activity Properties of Piper Species. *Molecules* **2022**, *27* (19). DOI: 10.3390/molecules27196774 From NLM Medline.

(23) Richards, L. A.; Oliveira, C.; Dyer, L. A.; Rumbaugh, A.; Urbano-Munoz, F.; Wallace, I. S.; Dodson, C. D.; Jeffrey, C. S. Shedding light on chemically mediated tri-trophic interactions: a 1H-NMR network approach to identify compound structural features and associated biological activity. *Frontiers in plant science* **2018**, 1155.

(24) Ampofo, S. A.; Roussis, V.; Wiemer, D. F. New prenylated phenolics from Piper auritum. *Phytochemistry* **1987**, *26* (8), 2367-2370.

(25) Snider, B. B.; Neubert, B. J. Syntheses of Ficuseptine, Juliprosine, and Juliprosopine by Biomimetic Intramolecular Chichibabin Pyridine Syntheses. *Org. Lett.* **2005**, *7* (13), 2715-2718. DOI: 10.1021/ol050931l.

(26) Roberson, M. G.; Smith, D. K.; White, S. M.; Wallace, I. S.; Tucker, M. J. Interspecies Bombolitins Exhibit Structural Diversity upon Membrane Binding, Leading to Cell Specificity. *Biophys J* **2019**, *116* (6), 1064-1074. DOI: 10.1016/j.bpj.2019.02.005 From NLM Medline.

(27) Richards, L. A.; Oliveira, C.; Dyer, L. A.; Rumbaugh, A.; Urbano-Munoz, F.; Wallace, I. S.; Dodson, C. D.; Jeffrey, C. S. Shedding Light on Chemically Mediated Tri-Trophic Interactions: A H-1-NMR Network Approach to Identify Compound Structural Features and Associated Biological Activity. *Front Plant Sci* **2018**, *9*. DOI: ARTN 1155 10.3389/fpls.2018.01155.